



## Research article

## Structural and mechanical characterization of custom design cranial implant created using additive manufacturing



Khaja Moiduddin <sup>a,\*</sup>, Saied Darwish <sup>a</sup>, Abdulrahman Al-Ahmari <sup>a</sup>, Sherif ElWatidy <sup>b</sup>,  
Ashfaq Mohammad <sup>a</sup>, Wadea Ameen <sup>a</sup>

<sup>a</sup> Princess Fatima Alhijris's Research Chair for Advanced Manufacturing Technology (FARCAMT Chair), Advanced Manufacturing Institute, King Saud University, Saudi Arabia

<sup>b</sup> Neurosurgery, Faculty of Medicine, King Saud University, Saudi Arabia

## ARTICLE INFO

## Article history:

Received 22 February 2017

Accepted 19 June 2017

Available online 28 June 2017

## Keywords:

3D modeling

Cranial reconstruction

Cranial tumor

Craniofacial reconstruction

Electron beam melting (EBM)

Fused depositing modeling (FDM)

Image-based surgery

Lighter implants

Mesh implant

Porous titanium

Traumatic bone destruction

## ABSTRACT

**Background:** Reconstruction of customized cranial implants with a mesh structure using computer-assisted design and additive manufacturing improves the implant design, surgical planning, defect evaluation, implant-tissue interaction and surgeon's accuracy. The objective of this study is to design, develop and fabricate cranial implant with mechanical properties closer to that of bone and drastically decreases the implant failure and to improve the esthetic outcome in cranial surgery with precision fitting for a better quality of life. A customized cranial mesh implant is designed digitally, based on the Digital Imaging and Communication in Medicine files and fabricated using state of the Art-Electron Beam Melting an Additive Manufacturing technology. The EBM produced titanium implant was evaluated based on their mechanical strength and structural characterization.

**Results:** The result shows, the produced mesh implants have a high permeability of bone ingrowth with its reduced weight and modulus of elasticity closer to that the natural bone thus reducing the stress shielding effect. Scanning electron microscope and micro-computed tomography (CT) scanning confirms, that the produced cranial implant has a highly regular pattern of the porous structure with interconnected channels without any internal defect and voids.

**Conclusions:** The study reveals that the use of mesh implants in cranial reconstruction satisfies the need of lighter implants with an adequate mechanical strength, thus restoring better functionality and esthetic outcomes for the patients.

© 2017 Pontificia Universidad Católica de Valparaíso. Production and hosting by Elsevier B.V. All rights reserved. This is an open access article under the CC BY-NC-ND license (<http://creativecommons.org/licenses/by-nc-nd/4.0/>).

## 1. Introduction

A cranial bone defect is caused by traumatic bone destruction, cranial tumor, congenital defects and result in functional and esthetic deficiencies. Craniofacial reconstruction is a complicated surgical process because it involves operating the body part which contains brain, eyes and other sensory organs, all within a confined space. The best way of treating cranial defects is by autogenous bone transplantation, as this will have fewer complications of infections when compared to implants from other materials [1]. However, their use is restricted due to the limited availability of suitable donor sites, especially for the large and complex defects, tissue harvesting problems, donor site morbidity and expensive surgeries. For this reason, implants from other materials are sought. Several biocompatible materials which are lightweight and non-carcinogenic such as

polyethylmethacrylate (PMMA), hydroxyapatite (HA) and Polyethylene are tried but each has its own individual shortcomings, such as risk of infections and lesser strength [2,3,4]. Currently, titanium, as in porous implants of different sizes, is the commonly used material for cranial reconstruction due to its excellent biocompatibility, customization and mechanical performance [5]. When titanium implant gets in contact with the body tissues, complex reactions takes place at bioenvironmental/oxide interface and a passive film forms on the titanium surface which is dense, protective, and adhere strongly to a substrate [6].

The ultimate aim of cranial bone reconstruction is to protect the brain and alleviate psychological affliction caused by the bone defect and to restore the appearance and psychological stability of the patient. The success of cranial reconstruction depends on the preoperative defect evaluation; implant design, material, and fabrication; and skills of the surgeon. Implant with a porous surface is considered more effective than rough coating [7]. Porous implant provides interfacial adhesion with the bone, leading to effective fixation and shorter healing time [8]. It should have high porosity with sufficient space for cell adhesion

\* Corresponding author.

E-mail addresses: [kmoiduddin@ksu.edu.sa](mailto:kmoiduddin@ksu.edu.sa), [kmoiduddin@gmail.com](mailto:kmoiduddin@gmail.com) (K. Moiduddin).

Peer review under responsibility of Pontificia Universidad Católica de Valparaíso.

and transportation of fluids. The ideal pore size for the bone ingrowth lies in the range of 500–1500  $\mu\text{m}$  [9]. Various researchers have revealed that porous titanium with a porosity of 50% is ideal for bone tissue ingrowth [9,10]. A porous structure having good interconnected pores results in significant bone ingrowth formation and in better implant fixation [11]. Although high porosity and pore size favor bone formation, a substantial increase of the same can diminish the strength of the implant. Hence the ability to produce a porous structure with controlled porosity through design and fabrication is a critical factor in the future clinical success.

In the past, several kinds of techniques have been employed in fabricating porous titanium and its alloys which include casting, fiber deposition and powder sintering [12,13,14]. However, all these processes have some kind of limitations, such as non-uniform porosity, impurities, and loose interconnections. Nevertheless, the ability to quickly and efficiently produce a patient-specific mesh implant has always been appealing from the manufacturing standpoint. One of the major developments in the medical industry is the adoption of Computer-aided design and Computer-aided manufacturing (CAD/CAM), and more recently additive manufacturing (AM) [10].

AM revolutionized the fabrication process in the medical industry with its unique technique of metal deposition using layer upon layer fashion. The advances of AM techniques have significantly improved the ability to prepare parts with precise geometries, using data from medical imaging, which is difficult while using traditional methods. The traditional method of manufacturing implants has many drawbacks, which include a compromise in the design and increase in production cost and time. Moreover, the implant doesn't match the requirement of bone contours and it involves manual bending and shaping by hand forming techniques [15]. In contrast, to match the bone contours and provide better cosmetic results, it is essential to use the concept of customized implant design using medical modeling software and its fabrication using freeform AM technologies. AM's strength lies in the areas where traditional methods reach their limitations with respect to "Customization". The AM technique can fabricate fully dense and graded structures with high precision and process flexibility. In recent years, cranial reconstruction implants are fabricated using AM and also these can be used as a template for producing the actual implant by the forming technique [16].

Electron Beam Melting (EBM) is one of the most recent and important technologies of AM. Researchers have identified EBM as one

of the major breakthroughs in the fabrication of customized porous titanium implants with controlled porosity [17]. EBM is a widely used technology for fabrication of medical implants in both Europe and America with an FDA (Food and Drug administration) approval [18]. Previous studies have proved EBM as a valid option for custom designed implants using titanium alloy in orthopedic, craniofacial and maxillofacial surgeries [19,20,21]. Cranial defects have been repaired in earlier studies using bulk titanium implants with 1.6 times more weight than the portion of the bone removed [22]. This bulky titanium implant introduces stress shielding effects at the implant-bone interface, because of the wide differences in the Young's modulus [23]. Young's modulus is considered as an important criterion to judge the suitability of the implant in medical reports [24]. Some researchers have tried reducing the stress shielding effect, by introducing porous structure in the cranial implants, but with no clear evidence and investigation on the behavior of the porous structure, porosity and its strength [17,25]. One of the important criteria for the success of a porous implant is its open and interconnected network of channels without any internal defects and its mechanical strength to withstand the desired load. In the present study, we have designed and fabricated a customized cranial mesh implant from CT scan with design validation. The designed mesh implant was investigated and evaluated based on its porous structure and mechanical strength.

## 2. Materials and methods

### 2.1. Medical image processing

A 38-year-old patient was referred to a craniofacial surgeon with a large cranial defect in the left parieto-temporal area. The patient was subjected to CT scanning and the resulting images were saved in DICOM (Digital imaging and communication field of medicine) format. Mimics 17.0® (Materialise NV, Belgium) software specially developed for image processing was used to convert the DICOM files into a typical 3D model. The obtained 3D model contains information about the patient's bones, skin, and soft tissues. Segmentation and region growing techniques were applied with a Hounsfield unit in the range of 310–2850 for the segregation of hard and soft tissues. The generated 3D model of the patient facial anatomy using Mimics® is illustrated in Fig. 1. The 3D model with tumor located on the left side

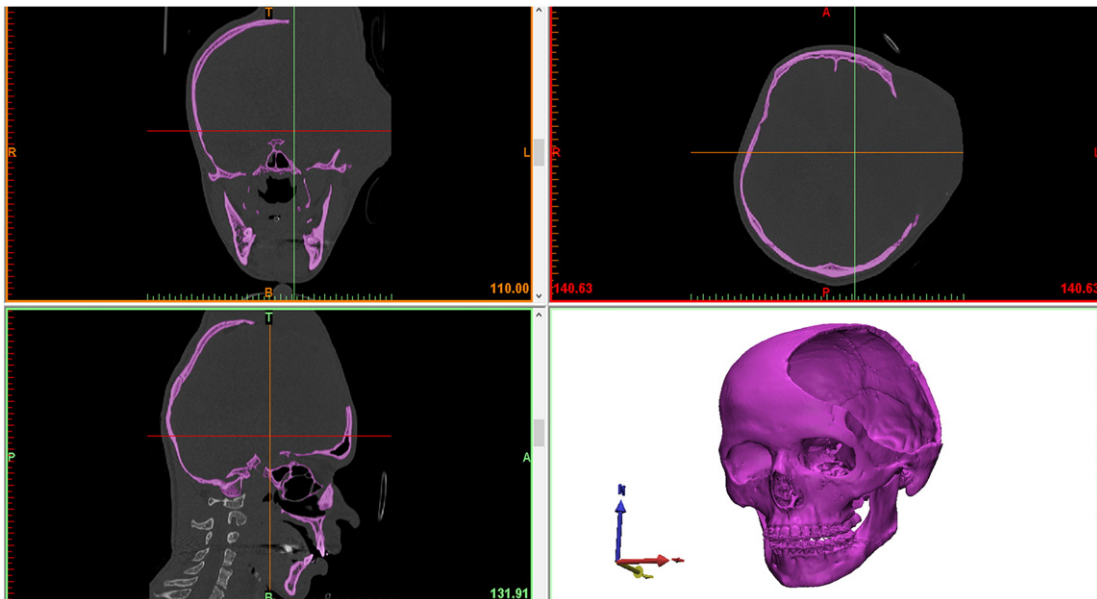


Fig. 1. 3D model of the patient's skull showing the tumor location on the left.

was saved as STL (Standard Tessellation Language) file for implant design process.

## 2.2. Customized implant design

The STL file of the 3D model (Fig. 2a) was imported in 3-Matic 9.0® (Materialise NV, Belgium) software to design a customized cranial reconstruction implant. The customized cranial implant was designed using mirror image reconstruction technique. In this technique, the skull was divided along the mid-plane by selecting two extreme endpoints (Fig. 2b). Afterward, the defective left side was cut and removed (Fig. 2c,d) and the contralateral side, the healthy bone was mirrored with reference to the mid-plane (Fig. 2e). Merging and wrapping operations were performed to overcome the gaps and discontinuous surfaces (Fig. 2f,g). Next, a Boolean operation (Fig. 2h) was performed between the newly developed skull model (Fig. 2g) and the old model that contains the tumor (Fig. 2a). This operation generates the customized cranial implant (Fig. 2i) with a thickness of ≈2.5 mm, the thickness of skull bone. An inward offset operation was performed on the implant design to reduce the thickness by half which is then used as a template, based on which the porous implant was built.

### 2.2.1. Porous implant design

The customized implant design obtained from the previous stage was a fully solid (bulk) design with a thickness of 1.25 mm. The four fixation lips with taper screw holes were designed for the firm attachment and fixation of the implant to the cranium as shown in Fig. 3b. The taper designed screw holes helps in the stability and rigidity with the complete sinking of the screws.

The bulk design file (Fig. 3a) was imported into Magics 18.03® structural module (Materialise NV, Belgium). Porous design cell type of body diagonals with nodes (Fig. 3d) from Magics® was patterned into the middle region (Fig. 3c). Fig. 3e illustrates the porous implant with the inner region as porous and the outer ends as bulk for fixing

of screws. The virtual assembly and validation of the implant design were performed by placing the mesh implant onto the skull model with a perfect fit, with little dead spaces as shown in Fig. 3f. The screw hole slots were tapered as shown in Fig. 3g, so that the screw heads can completely sink inside the holes, enhancing the patient comfort during implant service. The designed cranial implant has a porosity level of 49.81% with the strut size of 800 μm and pore size diameter of 700 μm. Designed porosity was calculated according to the following equation, where the volume parameters were obtained from STL files using 3-Matic®.

$$\text{Porosity}\% = \left( \frac{V_1 - V_2}{V_1} \right) * 100 \quad [\text{Equation 1}]$$

where  $V_1$  is the volume of the bulk implant and  $V_2$  is the volume of the porous implant.

### 2.3. Fabrication of designed cubes

It's important for the implants to be lighter in weight with good mechanical strength for better efficiency. The obtained cranial mesh design is lighter than the bulk implant by a porosity level of 49.81%. Cranial mesh implant due to its uneven and irregular structure cannot be subjected to any standard mechanical procedures. Hence, to study the mechanical strength of porous structure, a solid cube of 15 mm was designed and patterned with body diagonals node cell structure used in the cranial design as shown in Fig. 4. Few researchers have also performed similar work on porous titanium cubes with different structures, to study the mechanical properties and structural designs [26,27,28].

The STL model of the porous cube (Fig. 4b) was loaded into Arcam's EBM machine for fabrication. EBM produces complex 3D parts directly from STL file. EBM selectively melts the metal powder in a layer building fashion. Titanium powder (Ti6Al4V ELI) with the particle size of 50–100 μm was used in this study. The chemical composition of

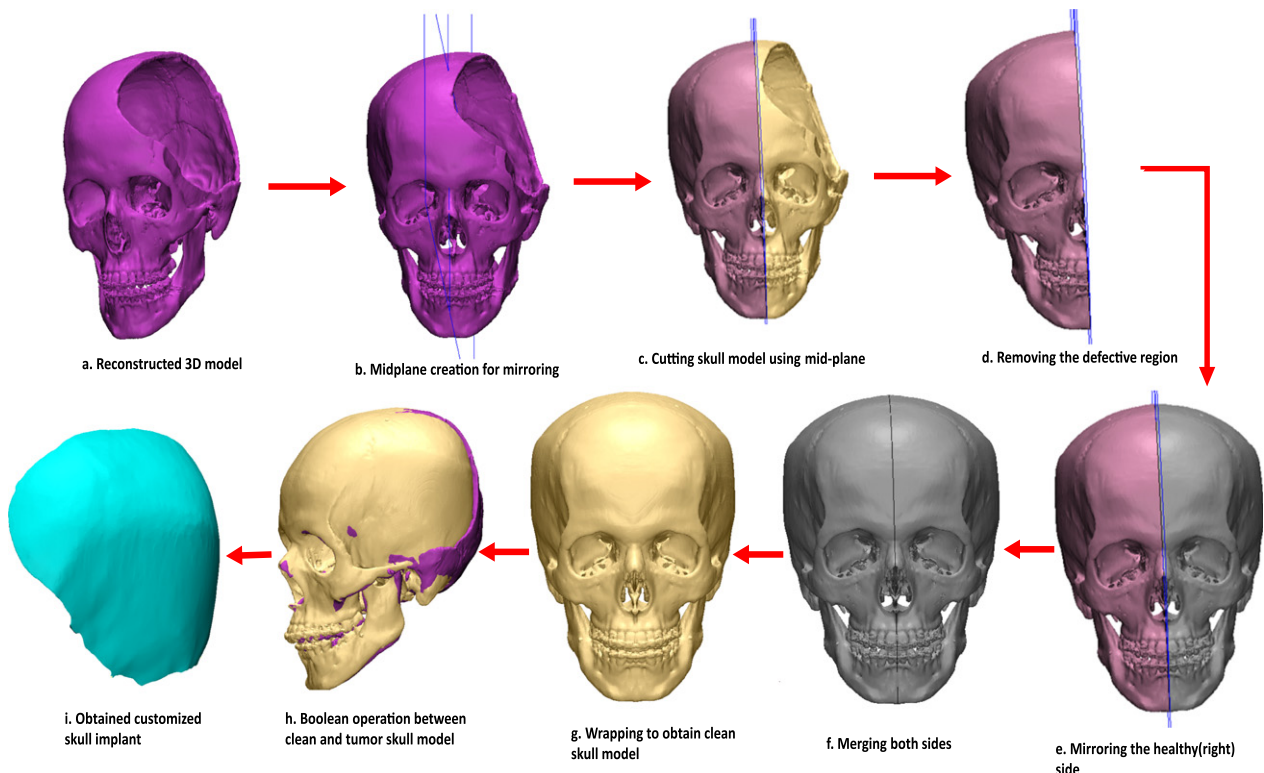


Fig. 2. Steps involved in the cranial reconstruction implant design using 3-Matic®.

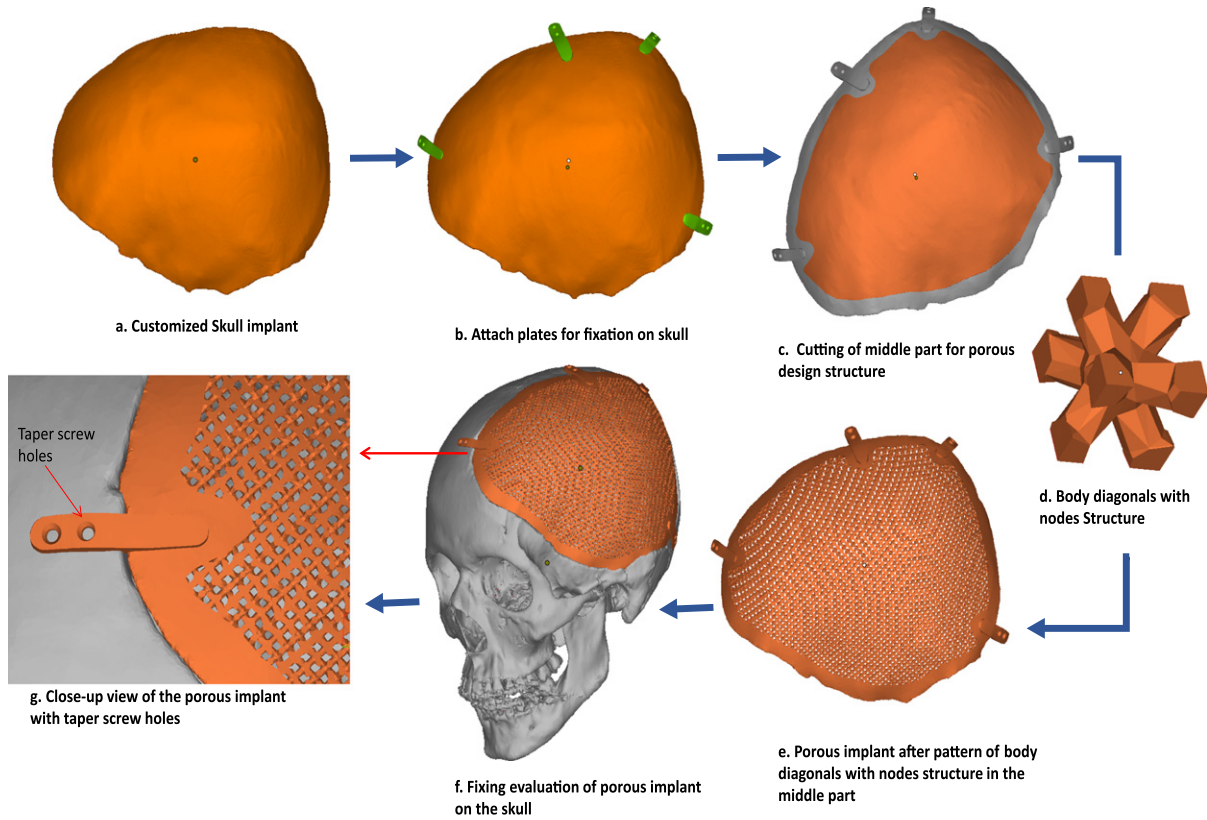


Fig. 3. Transforming cranial reconstruction implant from bulk to porous.

Ti6Al4V ELI (Extra low interstitial) was made of 6.04% Al (Aluminum), 4.05% V (Vanadium), 0.013% C (carbon), 0.0107% Fe (Iron), and 0.13% O (Oxygen), with the rest as Ti (Titanium) in weight percent. The schematic working principle of an EBM machine is illustrated in Fig. 5a.

The EBM process consists of three stages in general.

- Preheating the metal powder
- Scanning and melting the powder
- Lowering the build platform and raking the powder bed

**Stage 1:** The laid titanium powder in the powder bed was preheated by scanning the entire powder layer at high scan speed till the specified target temperature (730°C) was achieved. In preheating,

the powder layer was preheated to 80% of the melting temperature, which fuses the powder particles. Preheating is done to reduce the residual stresses and to sinter the loose powder to hold the subsequent next layer of powder. Standard Arcam parameters- preheat I and preheat II were used in this stage. In preheat I, the entire powder bed was scanned and in Preheat II, the scanning was performed only in the build area.

**Stage 2:** In scanning and melting stage, the high-velocity beam of electrons scans the metal powder line by line, by means of a magnetic lens, as per the defined CAD geometry. Scanning and melting operation consist of two stages, contouring and infill hatching. First, the contours were melted as per the boundary cross-section of the 2D slices by multiple electron beams. In

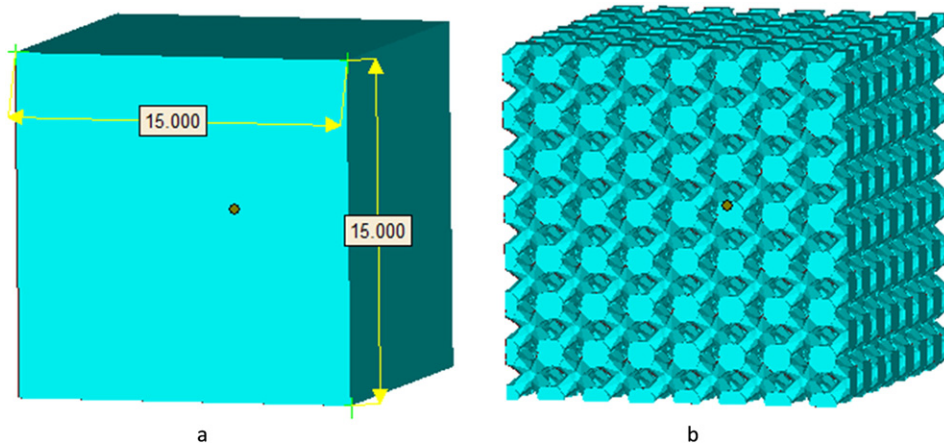


Fig. 4. Cubes with their structure unit cells of  $15 \times 15 \times 15 \text{ mm}^3$  (a) Solid, (b) porous structure with body diagonals with nodes cell type.

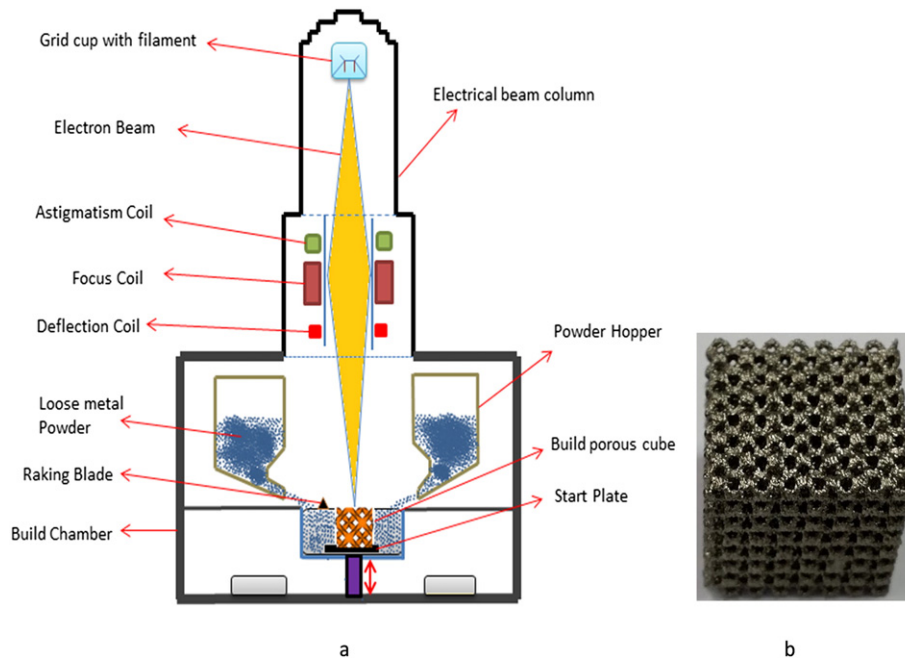


Fig. 5. (a) Schematic working of an EBM machine and (b) EBM produced porous cube.

hatching the beam current and the scan speed were increased when compared to contouring and was rastered in a snaking melt strategy in back and forth direction, to melt and fill the area between the contours. Only the contours and the hatching part, melts the metal powder and leave the rest of the powder untouched, which was recycled later.

**Stage 3:** After preheating and melting of each layer, the build platform was lowered by one-layer thickness ( $50\ \mu\text{m}$ ) and a new layer of powder was dispensed from hoppers and spread evenly onto the previously solidified layer using raking blades. These three stages were repeated in a cycle until the final three-dimensional physical parts were built.

The fabricated EBM porous cube as shown in Fig. 5b was then blasted in powder recovery system (PRS) with high-pressurized air mixed with Ti6Al4V ELI powder to remove the loosely trapped powder between the pores and the channels.

### 2.3.1. Structural characterization

In order to examine the structural integrity of the build porous cubes, they were subjected to micro-CT scans. Bruker Skycam 1173 scanner was used to detect any stochastic defects and to demonstrate the inner construction of the struts in the porous cube. A high resolution of the x-ray beam with a source voltage of 120 kV and a spot size of  $5\ \mu\text{m}$  was focused on the porous cube. Each 2D slice image in the form of  $512 \times 512$  bitmap as output data was collected. The surface and elemental analysis of the EBM built porous cube was done by scanning electron microscope (SEM) using JOEL JSM-6610LV electron microscope along with the attached energy dispersive spectroscopy (EDS).

### 2.3.2. Mechanical characterization

The strength of the porous implant is dependent on the porosity of the part. The compressive strength reduces with increase in porosity. The EBM produced cubes ( $n = 3$ ) were subjected to axial compression test to determine their mechanical strength. The compression test was carried out using an Instron universal testing machine (3385 H, United States) with a crosshead speed of 1 mm/min. The applied load and displacement data were continuously monitored and recorded in a

computer during the test for further analysis. Average compressive strength and modulus of elasticity of the porous structure were determined from the stress–strain curves, derived from the load–displacement data recorded during the compression test. The surface mechanical properties of the porous cube were determined by Vickers micro-hardness test using Buehler Micromet 5100-unit machine on the polished cubes with a load of 200 mgf and dwell time of 10 s. Three random areas were selected from the top surface of three porous cubes and an average value of 9 measurements was reported for hardness.

## 3. Results and discussion

### 3.1. Structural characterization results

The internal characterization results from the micro-CT scan of the EBM fabricated porous cube are illustrated in Fig. 6. They prove that the produced porous cubes are free from substantial internal defects such as cracks or voids and are interconnected with a series of network channels.

The EBM fabricated cube when subjected to Energy-dispersive X-ray (EDX) analysis, shows peaks corresponding to the various elements. As shown in Fig. 7, the titanium (Ti) peaks are more pronounced than the aluminum (Al) and vanadium (V) as expected.

The overall composition of the specimen is given in Table 1. Based on the composition results, it can be said that the chemical composition of the fabricated cubes did not differ much from the original composition of the feedstock powder.

The EBM fabricated porous cube subjected to SEM at low magnification after mechanical polishing. The SEM on the top surface of the cross-sectional porous cube (Fig. 8a) illustrates the microscopic image of one of the junctions as shown in Fig. 8b, where four struts meet. No major discontinuity and internal defects were found in struts or at their junctions.

### 3.2. Mechanical characterization results

The stress–strain relationship of the porous cube ( $n = 3$ ) was calculated and plotted as shown in Fig. 9. The compressive strength

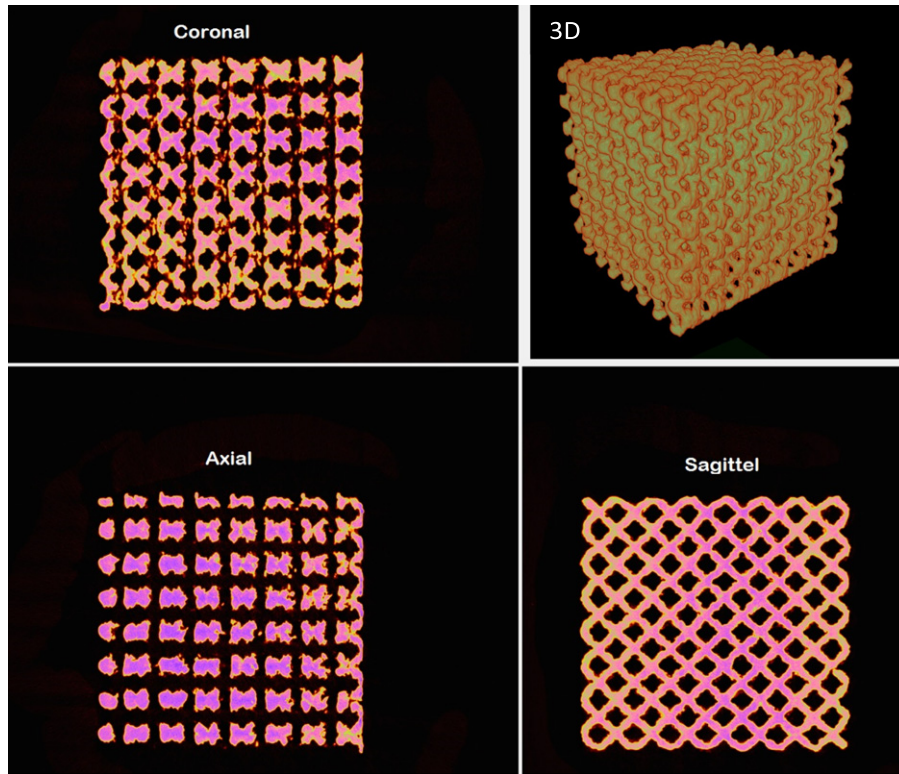


Fig. 6. Micro-CT scan images of the porous cube representing different cross-sectional views along with a 3D view.

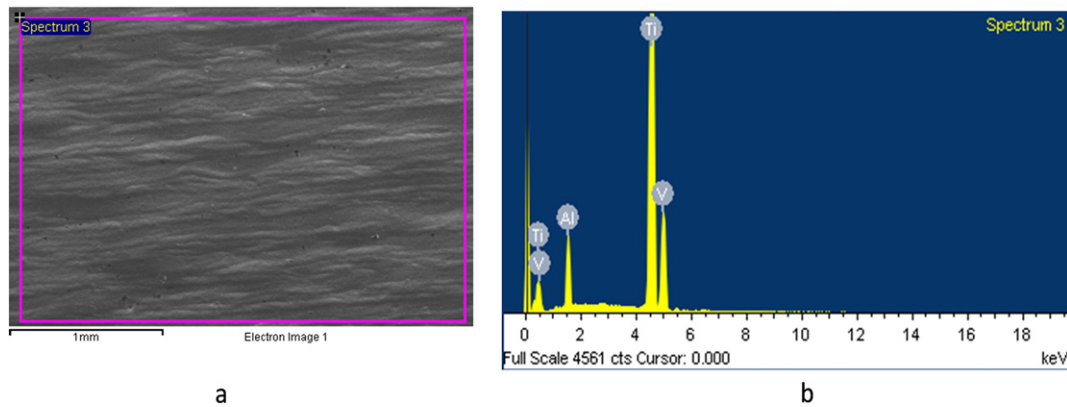


Fig. 7. (a) Scanning Electron microscopic image and (b) EDX Spectrum of EBM built Ti6Al4V ELI specimen.

and modulus of elasticity were derived from the stress–strain relationship curve. The maximum stress of 62.5 MPa in porous cube corresponds to the collapse of the individual layers with the thinnest struts collapsing first. The compressive strength of the porous cubes (62.5 MPa) is sufficient for the cranial reconstruction implants as these are non-load bearing implants. The porous cubes with modulus of elasticity of 1.20 GPa obtained from the stress–strain curve were closer and within the range of bone modulus of elasticity (1–20 GPa),

**Table 1**  
Quantitative EDX analysis results of EBM produced specimen.

Element	Weight %	Atomic %
Al	6.24	10.59
Ti	89.87	85.91
V	3.89	3.50

thus providing a promising means of stiffness reduction and stress shielding effect.

The micro-hardness test was performed on the porous cube, to study the material's resistance to deformation as shown in Fig. 10. The corresponding average hardness together with compression test results are displayed in Table 2.

The porous cubes resulted in higher average hardness of 343 HV in comparison to bulk part (310 HV [29]), a similar trend reported by other studies as well [30]. The higher hardness of porous structure is attributed to the high solidification rate of the porous struts when compared to the bulk cube.

#### 4. Fabrication of cranial implants

The customized cranial mesh implant was initially fabricated through polymer based fused deposition modeling (FDM) for rehearsal and

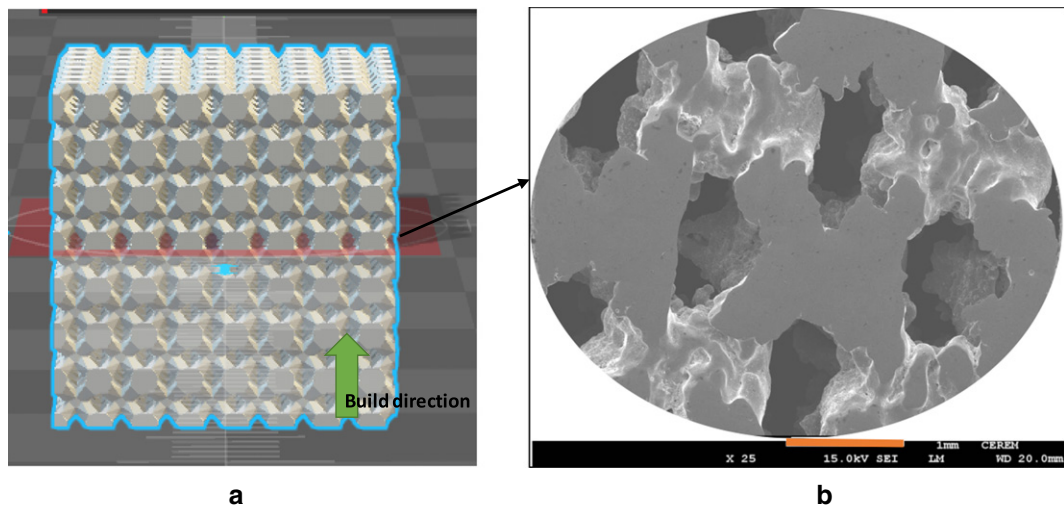


**Fig. 8.** (a) Cross-section of the porous cube and (b) SEM observation and distribution of micro-pores.

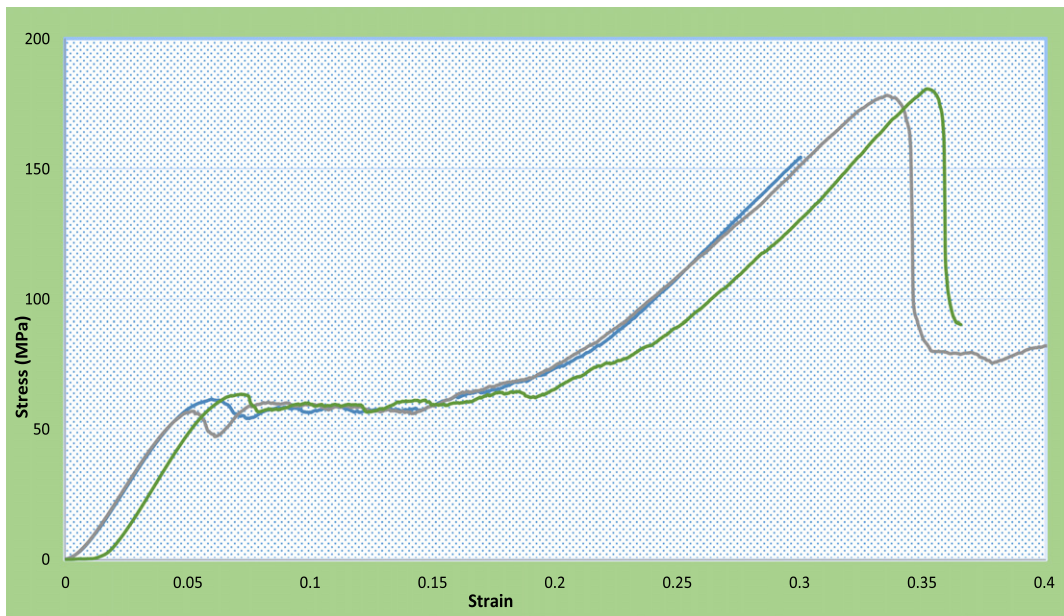


**Fig. 9.** Compressive stress–strain relationship curve of porous cubes.

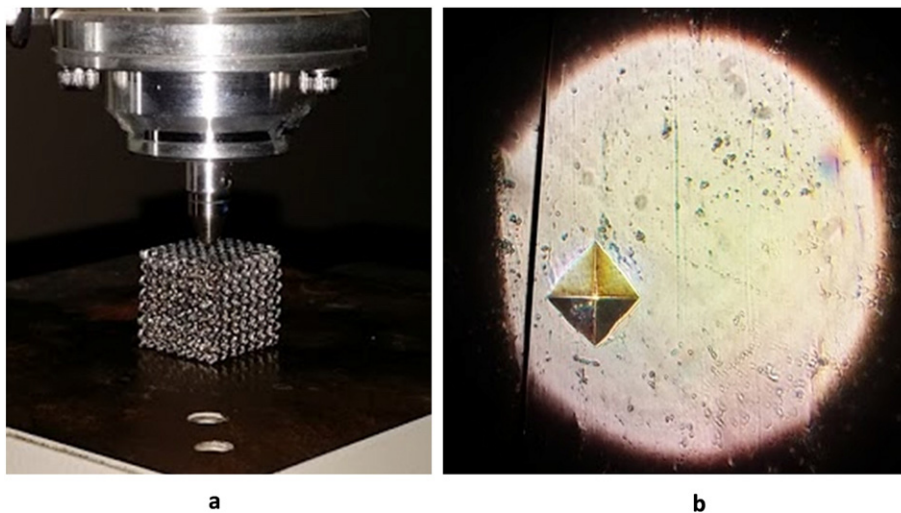


**Fig. 10.** (a) Vickers hardness test done on the porous cube and (b) indentation display on the cube.

**Table 2**  
Compression and hardness values of designed cubes.

Specimen	Average compressive strength (MPa)	Average modulus of elasticity (GPa)	Average hardness (HV)
Porous cube	62.5	1.20	343

fitting evaluation. If the polymer implant fails in fitting evaluation, due to the shrinkage effect and orientation of the build, the design process is repeated till the satisfactory results are achieved. Upon successful rehearsal and fitting evaluation, the final porous (Ti6Al4V ELI) implant was fabricated using EBM.



**Fig. 11.** (a) Stratasy FDM machine with produced parts, (b) Skull framework with the cranial implant and (c) Fitting evaluation of the cranial implant.

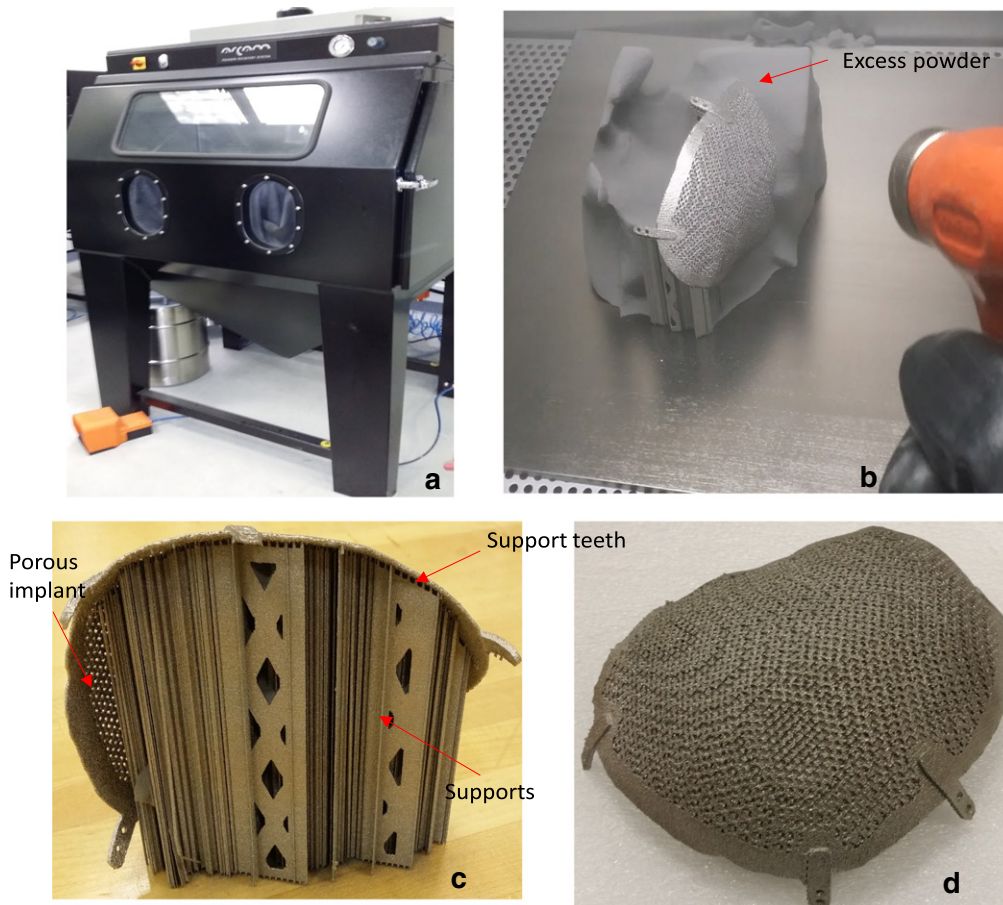


**Fig. 12.** (a) The PRS unit used for blasting excess powder, (b) Cranial implant inside the PRS unit, (c) Implant with supports with attached teeth and (d) implant after support removal.

#### 4.1. Polymer-based implant fabrication for rehearsal and fitting evaluation

The STL models of the customized implant design and the skull framework were imported into the Stratasys FDM machine for fabrication. FDM uses Acrylonitrile Butadiene styrene (ABS) plastic and polycarbonate material which provides strong, robust and functional parts for testing. The FDM produced skull framework and the implant were assembled for rehearsal and fitting evaluation as illustrated in Fig. 11. The polymer-based model(s), provides a comprehensive view of physical defects and the surgeon can plan accordingly based on pre-operative examination using both physical analysis and digital simulation. It helps the surgeons to make better-informed decisions during surgery, thus improving the surgical success and patient recovery. The polymer models also provide surgical guidelines and hands-on surgical rehearsal in precision drilling and best location of placement of screws, prior to surgery.

#### 4.2. Fabrication of titanium implant using EBM process

After successful fitting evaluation of polymer models, the cranial implant design was fabricated using Ti6Al4V ELI through EBM technology. Support structures were added to the implant during the EBM built, for allowing the heat transfer to prevent deformation and to assist the overhanging parts. The supports attached to the implant

are equipped with teeth at top and bottom for easy removal. The EBM produced cranial implant was passed through powder recovery system (PRS) to remove the excess powder particles (Fig. 12a,b). The blasted Ti powder was filtered and recycled for future use. Fig. 12c,d illustrates the cranial implant with support and after support removal.

The porous cranial implant after blasting was fitted with the polymer skull framework for a final rehearsal. The implant precisely fits inside the defective region with little dead spaces as shown in Fig. 13b,c,d. The porous structure is surrounded by a 10 mm bulk part, which provides strength to the implant while fixing screws. This new concept of customized cranial mesh design with design validations and fabrication using state of the art-AM technology reduces the waiting time and faster surgery, thus assisting the patients to resume their normal functionality more quickly.

#### 5. Conclusion

Implant with porous structures plays a crucial role in long-term stability and bone ingrowth formation. In addition to porous structure, the implants should have adequate mechanical strength with patient-specific geometry to ensure proper connection to bone tissue without any need of handcrafting during surgery. In this study, a custom designed cranial implant with porous structure was developed from the CT scan and fabricated using AM. The EBM produced

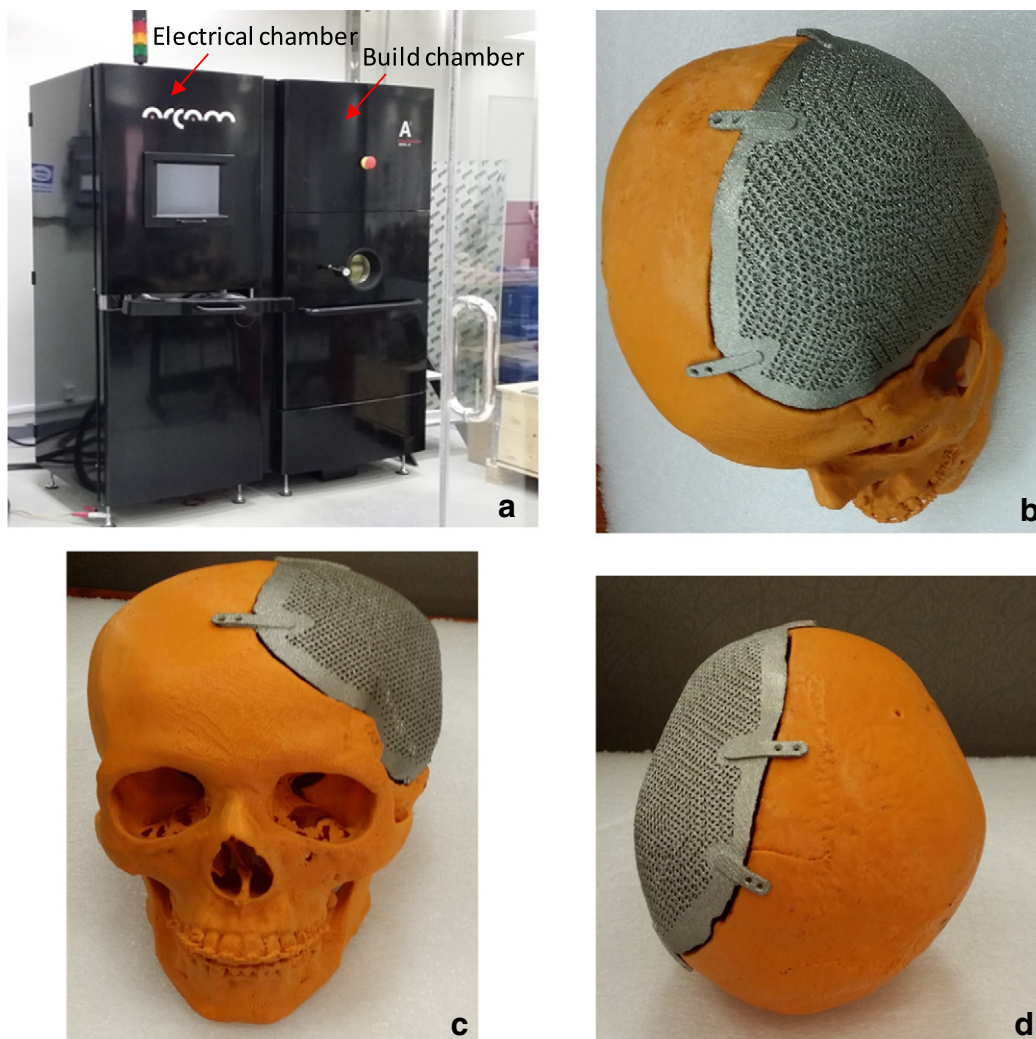


**Fig. 13.** (a) EBM A2 machine used for the fabrication of Ti6Al4V ELI porous implant, (b) Top view of skull framework with porous cranial implant, (c) Front view of skull framework with porous cranial implant, and (d) Back view of skull framework with porous cranial implant.

titanium mesh implant satisfied structural characterization with adequate strength. Moreover, the implant displayed a regular pattern of interconnected channels without any defects and voids. The use of customized cranial mesh implant, enhances the esthetic and functional rehabilitation of craniofacial deformities with faster healing and bone ingrowth formation and achieving immediate and efficient reconstruction.

### Conflict of interest statement

The authors have no conflict of interest to declare.

### Acknowledgment

The authors are grateful to the Deanship of Scientific Research, King Saud University for funding through Vice Deanship of Scientific Research Chairs.

### References

- [1] Elsalanty ME, Genecov DG. Bone grafts in craniofacial surgery. *Craniofacial Trauma Reconstr* 2009;2:125–34. <http://dx.doi.org/10.1055/s-0029-1215875>.
- [2] Durham SR, McComb JG, Levy ML. Correction of large (>25 cm<sup>2</sup>) cranial defects with 'reinforced' hydroxyapatite cement: technique and complications. *Neurosurgery* 2003;52:842–5. <http://dx.doi.org/10.1227/01.NEU.0000054220.01290.8E>.
- [3] Ducic Y. Titanium mesh and hydroxyapatite cement cranioplasty: a report of 20 cases. *J Oral Maxillofac Surg* 2002;60:272–6. <http://dx.doi.org/10.1053/joms.2002.30575>.
- [4] Engstrand T, Kihlström L, Lundgren K, Trobos M, Engqvist H, Thomsen P. Bioceramic implant induces bone healing of cranial defects. *Plast Reconstr Surg Glob Open* 2015;3(8):pe491. <http://dx.doi.org/10.1097/GOX.0000000000000467>.
- [5] Martin MP, Olson S. Post-operative complications with titanium mesh. *J Clin Neurosci* 2009;16(8):1080–1. <http://dx.doi.org/10.1016/j.jocn.2008.07.087>.
- [6] Wang G, Li J, Lv K, Zhang W, Ding X, Yang G, et al. Surface thermal oxidation on titanium implants to enhance osteogenic activity and *in vivo* osseointegration. *Sci Rep* 2016;6:31769. <http://dx.doi.org/10.1038/srep31769>.
- [7] Deporter DA, Watson PA, Pilliar RM, Chipman ML, Valiquette N. A histological comparison in the dog of porous-coated vs threaded dental implants. *J Dent Res* 1990;69:1138–45. <http://dx.doi.org/10.1177/00220345900690050401>.
- [8] Pilliar RM. Overview of surface variability of metallic endosseous dental implants: textured and porous surface-structured designs. *Implant Dent* 1998;7:305–14. <http://dx.doi.org/10.1097/00008505-199807040-00009>.
- [9] Otsuki B, Takemoto M, Fujibayashi S, Neo M, Kokubo T, Nakamura T. Pore throat size and connectivity determine bone and tissue ingrowth into porous implants: three-dimensional micro-CT based structural analyses of porous bioactive titanium implants. *Biomaterials* 2006;27:5892–900. <http://dx.doi.org/10.1016/j.biomaterials.2006.08.013>.
- [10] Lefebvre LP, Banhart J, Dunand DC. Porous metals and metallic foams. Proceedings of the fifth international conference on porous metals and metallic foams. DEStech Publications, Inc. 2008.
- [11] Nguyen HQ, Deporter DA, Pilliar RM, Valiquette N, Yakubovich R. The effect of sol-gel-formed calcium phosphate coatings on bone ingrowth and osteoconductivity of porous-surfaced Ti alloy implants. *Biomaterials* 2004;25:865–76. [http://dx.doi.org/10.1016/S0142-9612\(03\)00607-0](http://dx.doi.org/10.1016/S0142-9612(03)00607-0).
- [12] Erk KA, Dunand DC, Shull KR. Titanium with controllable pore fractions by thermo-reversible gelcasting of TiH<sub>2</sub>. *Acta Mater* 2008;56:5147–57. <http://dx.doi.org/10.1016/j.actamat.2008.06.035>.
- [13] Li JP, et al. Bone ingrowth in porous titanium implants produced by 3D fiber deposition. *Biomaterials* 2007;28:2810–20. <http://dx.doi.org/10.1016/j.biomaterials.2007.02.020>.
- [14] Chino Y, Dunand DC. Directionally freeze-cast titanium foam with aligned, elongated pores. *Acta Mater* 2008;56:105–13. <http://dx.doi.org/10.1016/j.actamat.2007.09.002>.
- [15] Samman N, Luk WK, Chow TW, Cheung LK, Tideman H, Clark RK. Custom-made titanium mandibular reconstruction tray. *Aust Dent J* 1999;44:195–9. <http://dx.doi.org/10.1111/j.1834-7819.1999.tb00221.x>.
- [16] Chen JJ, Liu W, Li MZ, Wang CT. Digital manufacture of titanium prosthesis for Cranioplasty. *Int J Adv Manuf Technol* 2006;27:1148–52. <http://dx.doi.org/10.1007/s00170-004-2309-y>.
- [17] Parthasarathy J. 3D modeling, custom implants and its future perspectives in craniofacial surgery. *Ann Maxillofac Surg* 2014;4:9–18. <http://dx.doi.org/10.4103/2231-0746.133065>.
- [18] FDA clearance. Arcam. Arcam announces FDA clearance of implants produced with additive manufacturing. Arcam AB. [cited February 18, 2017]. Available from Internet: <http://www.arcam.com/arcam-announces-fda-clearance-of-implants-produced-with-additive-manufacturing>.
- [19] Murr LE, Gaytan SM, Martinez E, Medina F, Wicker RB. Next generation orthopaedic implants by additive manufacturing using electron beam melting. *Int J Biomater* 2012. <http://dx.doi.org/10.1155/2012/245727>.
- [20] Al-Ahmari A, Nasr EA, Moiduddin K, Alkindi M, Kamrani A. Patient specific mandibular implant for maxillofacial surgery using additive manufacturing. International conference on industrial engineering and operations management (IEOM); 2015. p. 1–7. <http://dx.doi.org/10.1109/IEOM.2015.7093788>.
- [21] Mazzoli A, Germani M, Raffaeli R. Direct fabrication through electron beam melting technology of custom cranial implants designed in a PHANTOM-based haptic environment. *Mater Des* 2009;30:3186–92. <http://dx.doi.org/10.1016/j.matdes.2008.11.013A>.
- [22] Saldarriaga JF, Adolfo CP, Santiago CV, Carlos AT. Design and manufacturing of a custom skull implant. *Am J Eng Appl Sci* 2011;4:169–74.
- [23] Dujovne AR, Bobyn JD, Krygier JJ, Miller JE, Brooks CE. Mechanical compatibility of noncemented hip prostheses with the human femur. *J Arthroplasty* 1993;8:7–22. [http://dx.doi.org/10.1016/S0883-5403\(06\)80102-6](http://dx.doi.org/10.1016/S0883-5403(06)80102-6).
- [24] Niinomi M. Biologically and mechanically biocompatible titanium alloys. *Mater Trans* 2008;49:2170–8. <http://dx.doi.org/10.2320/matertrans.L-MRA2008828>.
- [25] Cho HR, Roh TS, Shim KW, Kim YO, Lew DH, Yun IS. Skull reconstruction with custom made three-dimensional titanium implant. *J Craniofac Surg* 2015;16:11–6. <http://dx.doi.org/10.7181/acs.2015.16.1.11>.
- [26] Wieding J, Jonitz A, Bader R. The effect of structural design on mechanical properties and cellular response of additive manufactured titanium scaffolds. *Materials* 2012;5:1336–47. <http://dx.doi.org/10.3390/ma5081336>.
- [27] Wu SH, et al. Porous titanium-6 aluminum-4 vanadium cage has better osseointegration and less micromotion than a poly-ether-ether-ketone cage in sheep vertebral fusion. *Artif Organs* 2013;37:E191–201. <http://dx.doi.org/10.1111/aor.12153>.
- [28] Mediaswanti K, et al. A review on bioactive porous metallic biomaterials. *J Biomed Mater Res* 2013;18:1–8. <http://dx.doi.org/10.4172/1662-100X.1000104>.
- [29] Kirchner A, Klöden B, Luft J, Weißgärber T, Kieback B. Process window for electron beam melting of Ti-6Al-4V. *Powder Metall* 2015;58:246–9. <http://dx.doi.org/10.1179/0032589915Z.000000000244>.
- [30] Murr LE, et al. Next-generation biomedical implants using additive manufacturing of complex cellular and functional mesh arrays. *Philos Trans R Soc Math Phys Eng Sci* 2010;368:1999–2032. <http://dx.doi.org/10.1098/rsta.2010.0010>.